Journal of
Advanced
Science and
Research

Contents available at:
https://www.swamivivekanandauniversity.ac.in/jasr/

Effect of annealing and hydrothermal temperature on the Structural and Optical Properties of Sol-Gel Dip Coated Titanium di-oxide Thin films

Sayari Biswas[1]; Kazi Hasibur Rahman[2]; Asit Kar[3]

[1,3] Micro and Nanoscience Laboratory, Department of Applied Physics, Indian Institute of Technology (Indian School of Mines), Dhanbad - 826004, Jharkhand, India.

[2]Swami Vivekananda University, Kolkata, India

Cite this article: Sayari Biswas; Kazi Hasibur Rahman; Asit Kar,2025, Effect of annealing and hydrothermal temperature on the Structural and Optical Properties of Sol-Gel Dip Coated Titanium di-oxide Thin films; Volume 1 (Issue 1): Pages 22-39.
DOI: 10.29322/IJSRP.X.X.2025.pXXXX

Received: 29. August 2024

Accepted: 30 November 2024

Published online: 15 March 2025

Keywords: TiO_2 thin film, autoclaved sol, hydrothermal method, dip coating.

Authors for correspondence:
Author Name: Sayari Biswas[1], Kazi Hasibur Rahman[2]
e-mail: [1]sayaribiswas@gmail.com
[2]via.kazi786@gmail.com

Abstract: Titanium dioxide (TiO_2) thin films were synthesized by sol-gel dip coating method on ITO coated glass substrate. The TiO_2 sol was prepared by hydrothermal method at two different temperatures – 90 ºC and 180 ºC. It was then used to deposit the films by dip coating method Afterwards half of them were annealed at 500 °C for 6 h and rest of them kept as deposited. XRD peaks confirm the of anatase phase formation for all the samples. Abrupt rise of transmission spectra was observed in the violet-ultraviolet transition region and a maximum value of ~40% was attained for as-deposited sample made from 90 °C sol. The prepared films consist of spherical nanoparticles. But they are not homogeneous in terms of thickness. So they exhibit varying RMS roughness when studied by AFM. Annealing and sol preparation temperature has a prominent effect on the surface roughness and also on the photocatalytic activity of the films.

1. Introduction:

For last few decades titanium dioxide (TiO_2) nanoparticles are attracting the researchers for its non-toxicity, cost effectiveness and unique physio-chemical properties. TiO_2 is a wide band gap n-type semiconductor. In general "Wide" band gap means a band gap value of at least 2 eV, significantly larger than that of the common semiconductors like silicon (1.1 eV) or gallium arsenide (1.4 eV). Due to its wide band gap nature, TiO_2 possesses interesting electronic properties along with the probability of easy nanostructuring and chemical stability. TiO_2 finds its usefulness in a variety of applications like dye-sensitized solar cell[1,2,3], photo catalysis[4], electronic device fabrication[5], energy storage[6], environmental purification[7], photo-induced water disinfection[8], , gas sensor[9], memory devices[10,11] etc. It has also the potential use in white pigment production[12], corrosion protective multilayer mirror[13], and antireflection coatings[14]. Due to enhanced surface are nanostructured TiO2 plays a crucial nanostructured TiO_2 plays a crucial role in improving the performance of several kind of devices.

TiO_2 has mainly three major crystalline phases: Anatase (tetragonal with a = 0.3785 nm, c = 0.9514 nm), Rutile (tetragonal with a = 0.4594 nm, c = 0.2958 nm) and Brookite (orthorhombic with a = 0.9184 nm, b = 0.5447 nm, c = 0.5145 nm)[15]. The anatase phase is developed, in general, at temperatures below 600 °C. At relatively higher temperatures (T > 600 °C), it is transformed into rutile. Previous studies show that, the morphology, crystal structure and stoichiometry of TiO_2 films are highly sensitive to deposition conditions like temperature and pressure, substrate type, substrate temperature etc.[16,17,18,19]. Thus optical properties of TiO_2 films, such as refractive index, extinction coefficient scattering losses etc. strongly depends on the deposition conditions.

So far, innumerable processes have been used for the formation of TiO_2 nano-structred materials like sol-gel method, hydrothermal and solvothermal methods, electrodeposition, electrochemical anodization, CVD, ALD, several template assisted routes etc. Negishi *et. al*. used diethylene glycol (DEG) and polyethylene glycol (PEG) as additives to prepare transparent TiO_2 thin films via sol-gel method [20]. Kasuga *et al*. adopted an alkali hydrothermal method to prepare titanate nanotubes without using any template[21]. Similarly several reports can be found for growth of TiO_2 thin film via CVD, ALD methods[22,23,24]. Karuppuchamy *et al*.[25] carried out cathodic electrodeposition dissolving $TiOSO_4$ powder in H_2O_2 solution. Ichinose *et al*.[26] have reported the preparation of peroxo-modified sol of anatase TiO_2 using peroxo-titanium acid (PTA) solution by the mixure of $TiCl_4$ and H_2O_2 solution. PTA sol is a economic way for making low-temperature (~100 °C) TiO_2 coating with high substrate adhesion and high transmittance. Lee *et al*.[27] prepared PTA sol using $TiCl_3$. In the present study PTA sol was hydrothermally treated to prepare the final sol for TiO_2 film deposition by dip coating method.

2. Method

2.1 Chemicals:

All the chemicals used in this work were of Reagent Grade. Titanyl sulphate [$TiOSO_4$], was used as the precursor. Other important chemicals used were Ammonia [NH_4OH, 3molL^{-1}] and Hydrogen peroxide [30% H_2O_2]. $TiOSO_4$ and NH_4OH were purchased from Sigma Aldrich and H_2O_2 was supplied by Avra Chemicals. ITO coated glass substrates were purchased from Macwin India Pvt. Ltd.

2.2 Synthesis:

TiO_2 thin films were deposited by dip coating method sing an Apex XDip-SV1 dip coater. The used for dip coating was synthesized via hydrothermal method at to different temperatures – 90 ºC and 180 ºC. To prepare the sol, first titanyl sulphate ($TiOSO_4$) was dissolved in distilled water at room temperature[28]. Next ammonia [NH_4OH, 3molL^{-1}] was added into this solution which results into the white precipitate of titanium hydroxide [$Ti(OH)_4$]. This white precipitate was collected in a filter paper and washed repeatedly with distilled water so that excess NH_4^+ and SO_4^- ions are removed. Then $Ti(OH)_4$, was homogeneously dispersed in distilled water and H_2O_2 (30%) was added in sufficiently under continuous magnetic stirring. After peptization for 20 h, Peroxo Titanic Acid (PTA) sol was obtained. Then the sol was put in a Teflon lined stainless steel autoclave and kept in a hot air oven for 12 h each. the process was repeated twice to prepare the sol at two different temperatures, viz. 90 ºC and 180 ºC. This final sol was used to deposit thin films by dip coating on ITO coated glass substrate. This particular substrate was choosen primarily to improve the adhesion of TiO_2 films. It may also find several applications in device fabrication. Dipping and lifting speeds were kept constant at 20 mm/min. Before film deposition, all the substrates were cleaned in an ltrasonic bath with acetone and isopropyl alcohol respectively. Samples were deposited with 12 coating cycles. After deposition, at first the films were dried at 60 ºC for 30 minutes in a hot air oven. Next they were annealed at 500 ºC in a furnace for 6 h. Samples were also kept as deposited as well for further studies.

2.3 Characterization:

X-ray diffraction (XRD) was used to std the crystallinity and phase identification of the samples in θ-2θ scanning mode using Bragg-Brentano configuration. The scan was run between 10° and 80° at 0.02° intervals with a PANlytical X'Pert ultra fast diffractometer with $CuK_{\alpha 1}$ (λ = 0.154056 nm) radiation..

To determine the defect levels in the synthesized TiO2 films, Photoluminescence emission spectra was recorded in the wavelength range 300 nm – 600 nm with an excitation wavelength of 260 nm on a Horiba-2500 Acton Fluorescence Spectrometer with a 150 W Xe lamp. Absorption and transmission spectra of the deposited films were collected using Agilent Cary 5000 UV-Vis spectrophotometer.

Morphological studies of the surface of the films were studied by FE-SEM Supra 55 and Dimension ICON Atomic Force Microscopy (Bruker). FESEM, AFM and UV-Vis spectrophotometry were done at the Central Research Facility, IIT (ISM) Dhanbad.

The photocatalytic activity of the prepared thin films were analyzed by decomposition of aqueous solution of Methylene Blue (MB) dye. Initially, 1.5×10^{-6} M Methylene Blue was added in to 100ml of DI water and stirred for 15 minutes. The TiO_2 thin films were placed inside the solution with the help of a copper holder and exposed under UV light. 5 ml of the solution was taken from the total solution at the regular interval of 15 min until a total duration of 90 min. UV-Vis absorbance spectra of the collected solutions were recorded with an Ocean Optics DH–2000–BAL UV-Vis spectrophotometer in the range 500 nm – 800 nm to evaluate the degradation rate of the dye.

3. Result and Discussion

3.1 Crystal Structure:

Fig. 1 shows the XRD profiles of the TiO_2 thin films with 12 numbers of coatings. For clarity we have shifted the profiles (b) – (d) along Y-axis with appropriate values.

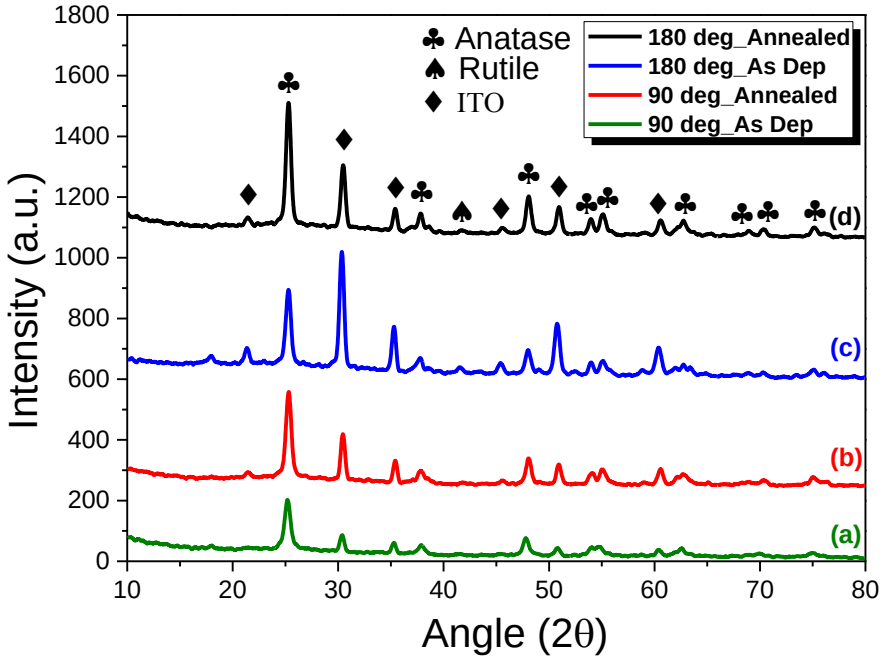

Figure 1: XRD profiles of samples made from 90 °C sol and 180 °C sol

The XRD peaks show that anatase phase is formed almost without any contamination of other phase of TiO_2 in all the samples. Only a very feeble peak appeared due to rutile phase (JCPDS 84-1285). Till date, several researchers have confirmed that, generally the anatase to rutile transformation takes place between 500 °C - 600 °C[29]. This explains the presence of anatase phase and appearance of small rutile peaks in the XRD patterns in annealed samples. But the rutile peak was also observed in the as deposited samples. The reason is not clear yet. Any amorphous background was absent in all of the patterns. This contradicts the observation made by Yuan and Tsujikawa[30]. They observed that, amorphous to crystalline transition for sol-gel derived anatase TiO_2 takes place in the temperature range of 200–300 °C. Most of the previous studies also found the as deposited films to be amorphous and even in some cases, low temperature calcinations (200 °C – 300 °C) did not improve this nature[31,32,33,34]. But in our study we found the films crystallized in anatase phase even in the as deposited conditions which has been very rarely reported yet[35,36]. During the synthesis process when the particle grows, if the involved atoms have sufficient energy, the atoms acquire enough mobility to position themselves to low energy positions leading to the formation of crystalline phases. High temperatures can achieve this condition. But in our case, this crystalline phase was achieved at comparatively low synthesis temperature. The sol for our thin films was made in an autoclave under high pressure. There are suggestions that high density negative oxygen ions are movable at high pressure which impart high energy to the atoms[37]. This may be the reason for crystalline anatase phase formation in as deposited condition in the present study.

To have more detailed information about crystallinity, the crystallite size was calculated from full width at half maximum (FWHM) of the XRD peaks (101), (004), (200), (105), (211), (204), (116), (220) and (215) using the Scherrer formula:

$$D = \frac{K\lambda}{\beta_{hkl}\cos\theta} \quad (1)$$

Here β_{hkl} is the peak width at half of maximum intensity (FWHM), K=0.94, λ is wavelength of the incident X-ray = 0.1542 nm and D is the crystallite size. Thermal treatment to the sol increases the crystallite size. For samples prepared from 90 °C sol crystallite size was found to be 14 nm and 17.4 nm for as deposited and annealed films respectively. For samples made from 180 °C sol, the values are 16.8 nm and 18.3 nm respectively. For the second case, i.e. relatively higher sol preparation temperature introduces bigger nanocrystals. Similarly, annealing also has an effect on crystallization of the films. Crystallite size increases as a result of relaxation of grain boundaries due to increased thermal energy. Any other forms of Ti oxides such as Ti_3O_5, Ti_2O_3, and TiO were undetected.

3.2 FESEM:

Figure 2 shows FESEM images of the films, prepared from both the sols (90 °C and 180 °C). Irrespective of sol preparation temperature all the samples consist of spherical or almost spherical particles. During film deposition, when the substrate is dipped into the sol, TiO_2 particles get attached to the substrate and during the drying process it forms the film. The sols were prepared by hydrothermal method. During the hydrothermal process the spontaneous nucleation leads to aggregation of crystallizing particles and in our case it takes the spherical or almost spherical shape.

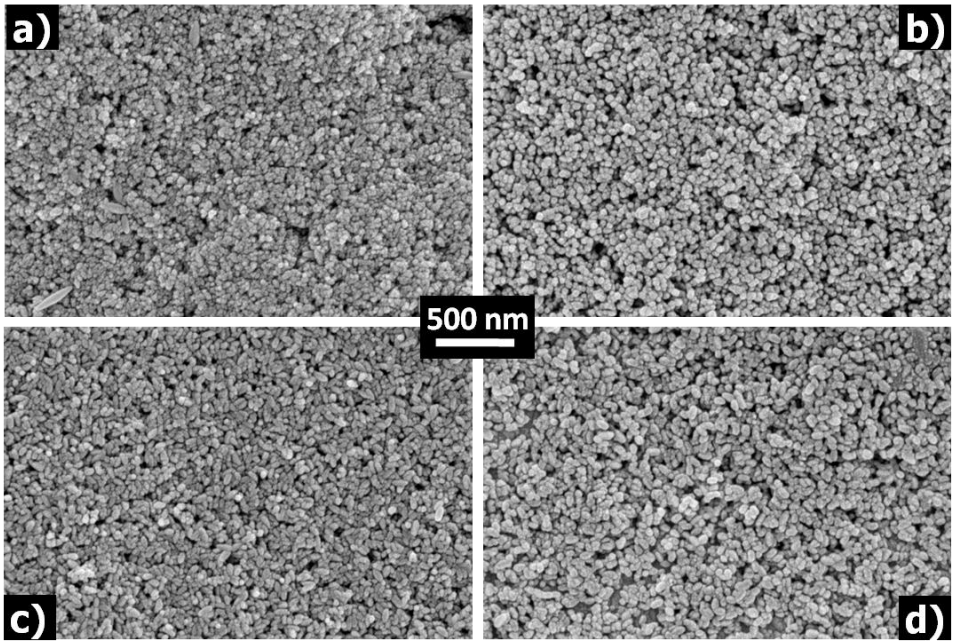

Figure 2: FESEM areal view of (a) as deposited sample made from 90 °C sol (b) annealed sample made from 90 °C sol (c) as deposited sample made from 180 °C sol (d) annealed sample made from 180 °C

Generally, during particle formation it takes the shape (in nano regime) where it acquires minimum free energy. Spheres have minimum surface area for a given volume. The spherical shape of the particles minimizes the surface energy in the given thermal condition. Our samples were prepared in hydrothermal system i.e. under high pressure. Thus the volume growth is restricted from all sides. It also leads to the formation of spherical particles. Although some of them show a little elongated shape which happens due to the spatial restrictions because of their as the closely packed nature.

Spherical microstructures are distributed homogeneously on the film surface for all the samples. For the films made from 180 °C sol larger particles were observed. But comparing as deposited films made from both the sols, it was observed that the particle size increases when the hydrothermal temperature for sol preparation increases or when the samples were annealed. In this case, the thermal energy of the system increases due to increased sol preparation temperature and as an effect of annealing too. The grain boundaries then grow to compensate it. Crystallite size determined from XRD profile also supports the result revealing increment in crystallite size. Size increment as an effect of annealing is more prominent for samples made from 180 °C sol. When oxide molecules assemble into crystalline form, they need enough energy to overcome the activation energy required for the synthesis process. The increase in temperature is the simplest way to input energy into the system. When the temperature in the system is raised sufficiently,

it allows the molecules to gain more freedom. Therefore, they are able to reorganize themselves to grow bigger. This reorganization mostly happens at the expense of smaller particles. The smaller particles have the larger surface to volume ratio. Due to their higher surface area, it is more likely they will dissolve (melt) as they are treated to sufficiently high temperature. This dissolves (or melts) mass and then gradually deposits them on the crystals that remained, i.e. the larger ones. Thus the larger crystals grow even larger and the smaller ones disappears gradually leading to a uniform size distribution. Thus annealing also brings uniformity in the shape of the TiO_2 particles. Since 90 °C samples have lower particle size, the film surface is more even than 180 °C samples. With increasing sol preparation temperature, presence of some small voids was observed in all the samples. These voids appeared due to the increment in particle size and layered structure of the films. Smaller particles easily get fitted into the interstitial voids of the previous layer. But for larger particles, the interstitial sites are not enough. So, they tend to sit on the particle sites of the previous layers. That's why, in the samples made from 180 °C sol, void are more prominently observed in FESEM images. These voids provide additional effective surface area.

3.3 AFM Study:

The surface morphology and topography of the deposited films were studied by an Atomic Force Microscope (Dimension Icon) using contact mode. Two-dimensional (2D) and three-dimensional (3D) AFM images are shown in figure 3. 3D images show that the surface of the TiO_2 films has the shape of hills and valleys. 2D images reveal that (not shown here) the films have nanocrystalline granular morphology and TiO_2 particles are uniformly distributed all over the surface.

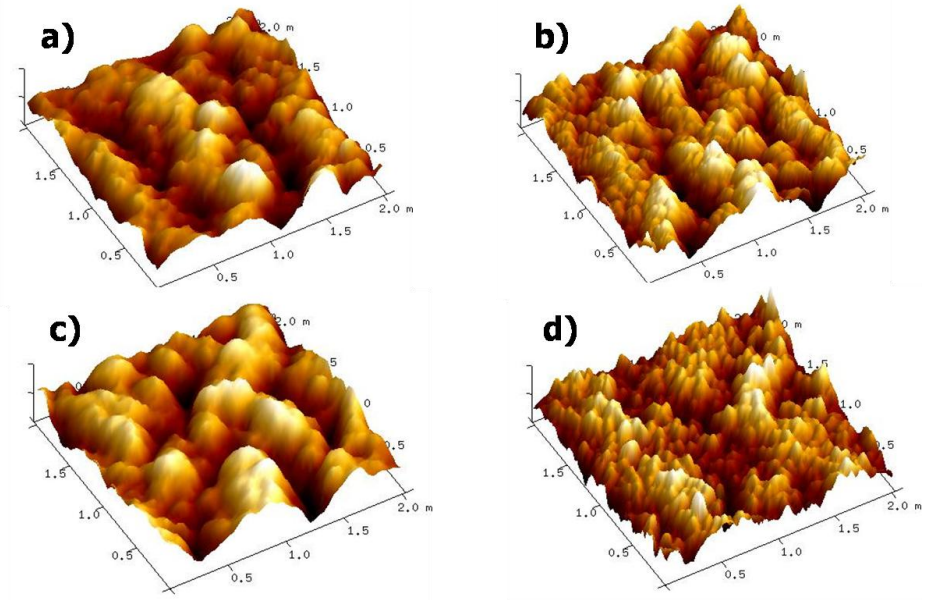

Figure 3: AFM 3D images showing the surface profile of (a) as deposited sample made from 90 °C sol (b) annealed sample made from 90 °C sol (c) as deposited sample made from 180 °C sol (d) annealed sample made from 180 °C

The films were mainly made of spherical particles. The surfaces of the films exhibited a certain degree of roughness and became rougher when the annealing temperature increases. For better understanding of the surface topography a variety of scans were carried out at random locations on the film surface keeping the scanned area constant at 2 μm × 2 μm. Obtained data were converted into NanoScope Analysis software (Version 1.4) to analyze different parameters like the root mean square roughness (R_q), average roughness (R_a), surface skewness (R_{sk}) and kurtosis (R_{ku}).

Surface roughness is a measure of irregularity or unevenness on the surface and provides a measure of how smooth (or rough) the surface of a film is. The measure of surface roughness is the vertical deviation from a standard surface or mean surface. Generally, the surface roughness is expressed in terms of two quantities ─ the root mean square or RMS roughness (R_q) and the average roughness (R_a). Average roughness (R_a) is the arithmetic mean of the measured absolute height of the surface with respect to a reference plane, calculated over the entire scanned length/area. Although it gives a good general idea about the height distribution of the scanned surface, R_a cannot differentiate between peaks and valleys, nor does it give any information about the spatial structure. A surface with high hills and deep valleys or with general isotropic morphology may yield the same average roughness value. Here comes the need

of RMS roughness. Root mean square roughness (R_q) is the standard deviation of the surface height distribution with respect to the mean surface and is considered to be more sensitive than the average roughness for visualization of surface properties. R_a and R_q can mathematically be explained according to the following equations[38]:

$$R_a = \frac{1}{L}\sum_{i=1}^{n} |z_i| \ \left(\text{or}, = \frac{1}{L}\int_0^L |z(x)| dx \right) \quad (2)$$

and

$$R_q = \sqrt{\frac{1}{L}\sum_{i=1}^{n} |z_i|^2} \ \left(\text{or}, = \sqrt{\frac{1}{L}\int_0^L |z(x)|^2 dx} \right) \quad (3)$$

Where L is the length of the profile on the x-axis used for measurement and z(x) is the height variation from the profile line for each data point.

The roughness of the prepared samples varies with sol preparation temperature. Post-deposition thermal treatment (annealing) also affects the film roughness. For samples prepared from 90 °C sol with 12 coatings, RMS roughness was observed to be ~47 nm and ~22 nm for annealed and as-deposited samples respectively. For the similar kind of samples, R_q increases to ~76 nm and ~34 nm when the sol preparation temperature is increased to 180 °C. The values of average roughness for the mentioned samples are ~37 nm, ~17 nm, ~60 nm and ~27 nm respectively. R_q values for all the samples are higher than R_a values which are justified by their definitions. Sample roughness (both R_a and R_q) increases after annealing. This increment might be a result of bigger particle size and improved crystalline nature of the films. Annealing at high temperature leads to an increase in mobility of atoms. It causes the agglomeration of particles and makes the particles bigger which in turn leads to increased roughness of the film as shown by previous studies[39,40]. Lin et al[41] described that the high temperature can hasten the migration of grain boundaries resulting in the coalescence of grains.

If the roughness profile follows a Gaussian distribution R_a and R_q are interchangeable:

$$R_q \approx \sqrt{\frac{\pi}{2}} R_a \approx 1.25 \times R_a \quad (4)$$

i.e., according to the statistical theory, the ratio of R_q to R_a should be 1.25, for Gaussian distribution of surface particles[42,43]. Ward[44] noticed that most of the engineered surfaces possess approximately a Gaussian height distribution with R_q/R_a values of up to 1.31. As shown in Table 1, the values of R_q/R_a for the present samples are reasonably close to 1.25, as predicted by the theory. This result significantly indicates a Gaussian height distribution of the film surfaces, at the imaging scale.

Besides surface roughness, we also evaluated the surface skewness and kurtosis. The definition of surface skewness (R_{sk}) is as follow[45,46],

$$R_{sk} = \frac{1}{R_q^3}\frac{1}{N}\sum_{i=0}^{N} Z_i^3 = \frac{1}{R_q^3}\int_{-\infty}^{+\infty} z^3 f(z) dz \quad (5)$$

Skewness is a dimensionless quantity, which in general is evaluated as positive or negative values and evaluates the symmetry of surface distribution. For negative skewness, the valleys are dominant over the scanned area, and the peaks are dominant when it is positive[46]. Our samples are valley dominant as all of them possess negative skewness values.

Kurtosis (R_{ku}) is mathematically directly related to the peak heights and valley depths according to the following formula[46]:

$$R_{ku} = \frac{1}{R_q^4}\frac{1}{N}\sum_{i=0}^{N} Z_i^4 = \frac{1}{R_q^4}\int_{-\infty}^{+\infty} z^4 f(z) dz \quad (6)$$

Where Z is the profile height at point number i. Kurtosis value projects an idea about the shape of the surface height distribution. When R_{ku} value for a surface is below three, it indicates that the scanned area has relatively less numbers of high peaks and low valleys, indicative of a bumpy surface. When R_{ku} is greater than three, the surface will have higher numbers of high peaks and deep valleys, characterizing a spiky surface. All our samples appear to follow the first case which is also evident from the AFM 3D images[47].

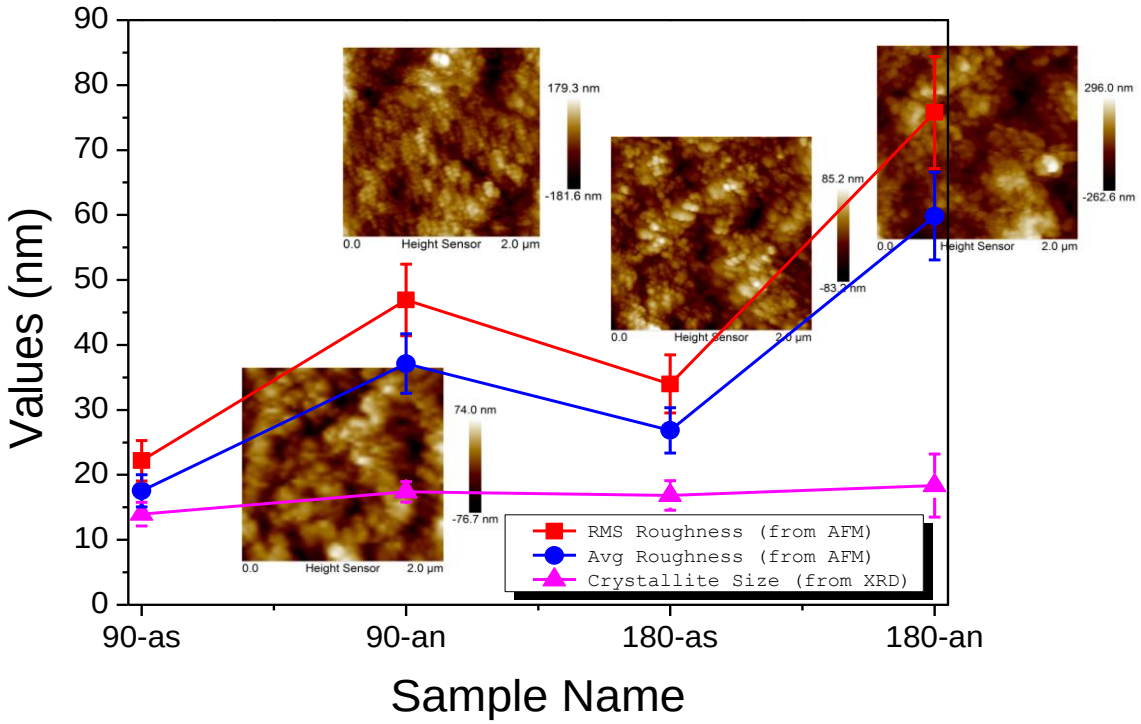

Figure 4: Graphical representation of (a) RMS roughness and (b) Average roughness and (c) crystallite size of the TiO_2 thin films obtained from AFM data and XRD profile

The Kurtosis values for the samples also indicates Gaussian distribution of surface profile, as mentioned earlier as well.[55]
R_a, R_q, R_{sk} and R_{ku} values of the samples are summarized in the following table1:

Sample Name	R_q in nm	R_a in nm	R_q/ R_a	R_{sk}	R_{ku}	Grain Size (nm)
90 deg-as dep	22.17	17.54	1.264	-0.22674	0.27077	13.9
90 deg-annealed	46.91	37.13	1.263	-0.10481	0.14984	17.4
180 deg-as dep	34.00	26.85	1.266	-0.19173	0.39181	16.8
180 deg-annealed	75.77	59.83	1.266	-0.09158	0.16708	18.3

For convenience, the table also shows the grain size of each sample which was obtained from XRD analysis. These values of RMS roughness, Average roughness and grain size has been graphically represented in **Figure 4**.

3.4 Optical properties:

Figure 5 shows the transmittance spectra of the deposited samples. Thin films show a gradual rise in transmittance starting at the violet-ultraviolet transition region from almost zero to maximum of ~40% at the near Infrared. This maximum transmittance value was observed for as-deposited sample made from 90 °C sol and it decreases with increased sol preparation temperature and annealing.

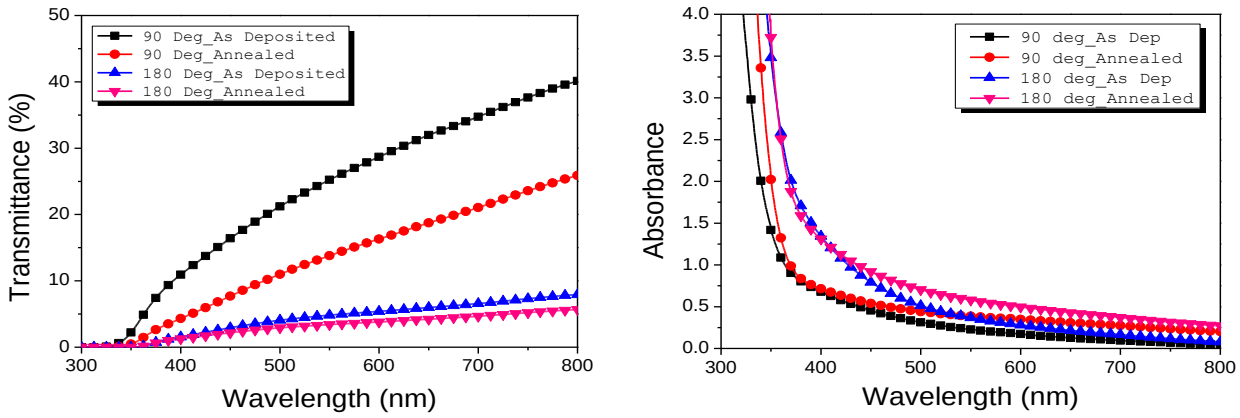

Figure 5: Optical Transmittance and Absorbance Spectra of as deposited and annealed samples made from both 90 °C sol and 180 °C sol

FESEM images reveal that, particle size increase with annealing and this eventually increase the amount of scattered light. Film uniformity reduces with increased sol preparation temperature and also after annealing enhancing amount of scattered light. The loss of light due to scattering and absorption results in decrease in the transmittance. In short enhancement of both absorption and scattering loss is the result of increased surface roughness as indicated by AFM studies. The transmittance edge slightly shifts towards longer wavelength as an effect of annealing and higher sol preparation temperature. In general, the scattering loss and the surface roughness have an exponential relationship[48]. Additionally at higher sol preparation temperature, presence of a large number of oxygen vacancies absorbs the incident light[49,50] which leads to decrease in transmittance.

The optical band gap (E_g) of the TiO_2 films was calculated using the following relation;

$$(\alpha h\nu)^{1/2} = \text{const.} \times (h\nu - E_g) \quad (7)$$

Where α is the absorption coefficient. Figure 6 depicts the relationship between $(\alpha h\nu)^{1/2}$ vs photon energy $h\nu$ of the TiO_2 films. The optical band gap of the films was determined by extrapolating the linear portion of the curves to the energy axis. For as deposited film made from 90 °C sol the value was found to be 3.24 eV. For the same film annealed at 500°C, the value was the same (3.22 eV). For the films made from 180 °C sol, the values are 3.13 eV and 3.08 eV respectively. The band gap decreased for when sol preparation temperature was increased, but for the film made from the same sol there is no considerable change in the band gap value. This is due to larger particle size and thermal stress in the films at higher sol preparation temperature. The increase in particle size is clearly observed in the FESEM images. In a single atom, the optical band gap is equal to the energy difference between the ground state and the first excited state. But in bulk, both levels get broadened forming a band. As particle size increases, broadening of bands also becomes greater decreasing the separation between the lowest of the conduction band and the top of the valence band. And this indicates the lowering of band gap energy.

The Urbach Energy values for all the samples were determined using Urbach's empirical rule,

$$ln\alpha = ln\alpha_0 + \frac{h\nu}{E_u} \quad (8)$$

The slope of the linear portion of lnα vs. hν gives us the Urbach Energy values. The calculated values were 275 meV, 218 meV, 306 meV and 251 meV for samples 90-as, 90-an, 180-as and 180-an.

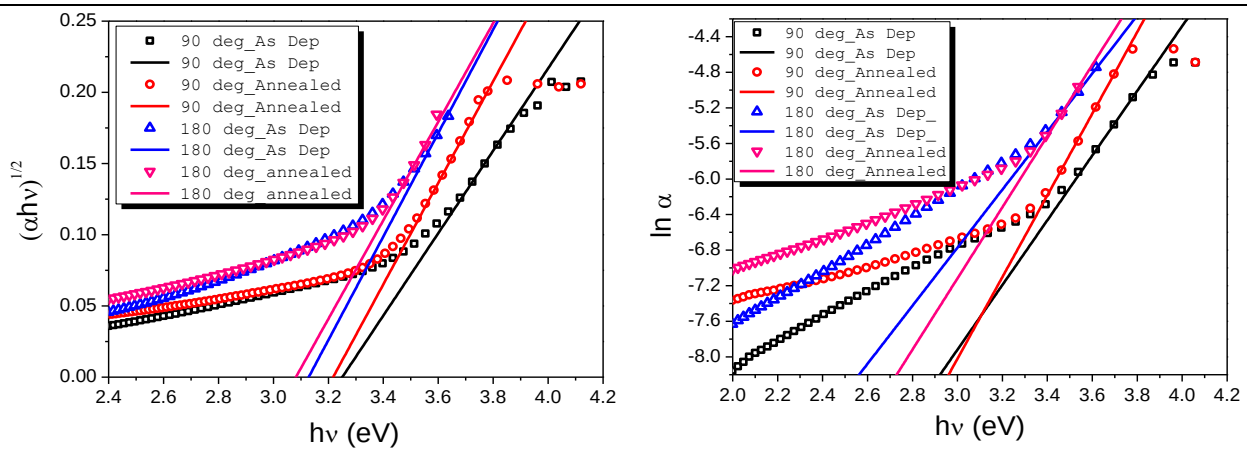

Figure 6: Band Gap determination from absorbance spectra of (a) samples made from 90 °C sol and (b) samples made from 180 °C sol

Urbach energy values are slightly larger in case of samples made from higher temperature sol. It means more energy level due to the disorderedness smears into the band edges causing the observed narrowing of band gap values. Annealing effect decreases Urbach Energy values indicating better crystallinity. This fact has also been supported by XRD studies. But after annealing this energy value decreases. Since the annealing process was carried out in ambient condition, number of oxygen vacant states reduced by the ambient oxygen. This was later confirmed by PL studies as well. In general oxygen vacancy defects create additional localised defect states which effectively influence the valence and conduction band edges causing the Urbach tail. So decrease in their numbers reduces the value of Urbach Energy.

Refractive indices and the extinction co-efficient of the deposited films were also calculated using the following formulae[51],

$$n = \frac{1+\sqrt{R}}{1-\sqrt{R}} \quad (9)$$

And[52]

$$k = \frac{\alpha\lambda}{4\pi} \quad (10)$$

Both the refractive indices and extinction co-efficients show exponentially decreasing nature throughout the observed wavelength range. The spectral dependence these parameters are shown in figure 7.

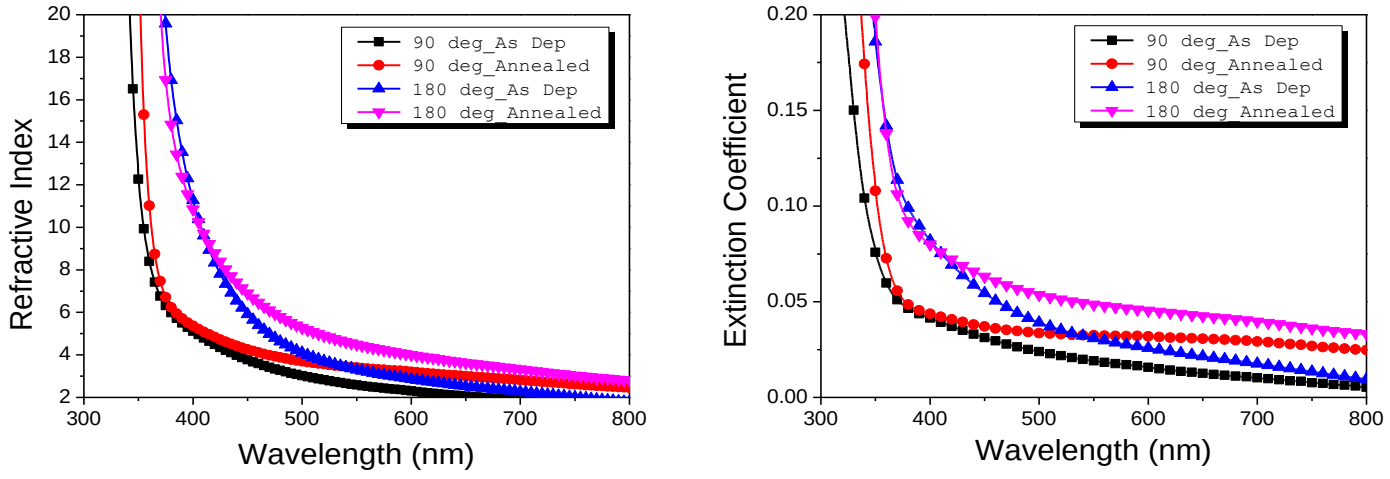

Figure 7: Refractive Index and Extinction Co-efficient of as deposited and annealed samples made from both 90 °C sol and 180 °C sol

In the lower wavelength region (i.e. higher incident energy) due to resonance phenomenon between the incident electromagnetic radiation and the electron polarization in the material coupling of electrons take place. This leads to attenuation in propagation of electromagnetic wave through the material. Thus, both refractive index and extinction coefficient showed higher values at lower wavelength region. Refractive index values were observed to increase with increase in sol preparation temperature and also with

annealing. This is due to improved packing density and crystallinity of the films as a result of annealing. In the as deposited films lower molecular mobility leads to loosely packed TiO2 particles. Any additional thermal energy increases the mobility and packing density as well leading to refractive index increment. Annealing in atmospheric condition allows the material capture oxygen from the environment decreasing the number of oxygen vacancies which was later confirmed by PL studies. This is another reason for increase in refractive index after annealing. Extinction coefficient also exhibited a similar trend like refracrtive index. Increase in film roughness due to thermal treatment leads to results into more scattered light from the surface. Thus extinction coefficient also increases with annealing.

The obtained values of n and k were used to calculate both real ε_r and imaginary parts ε_i of the dielectric constant and they were obtained using the formulas[52]:

$$\boldsymbol{\varepsilon_r = n^2 - k^2} \quad \textbf{(11)}$$

$$\boldsymbol{\varepsilon_i = 2nk} \quad \textbf{(12)}$$

The variation of both real ε_r and imaginary ε_i parts of the dielectric constant with the incident wavelength for all TiO_2 samples are shown in Figure 8.

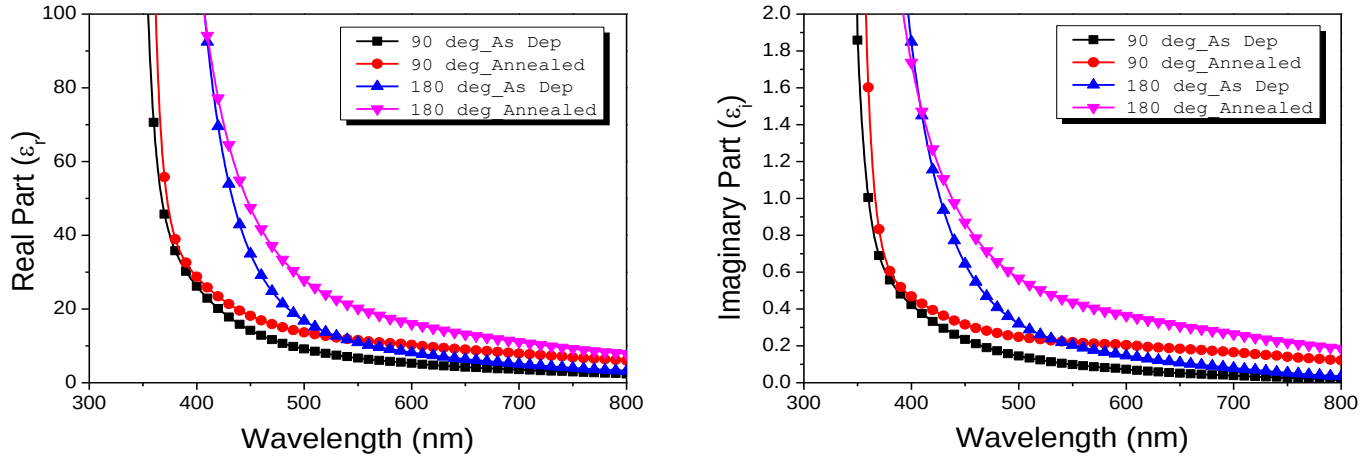

Figure 8: Real and Imaginary part of the dielectric constants of as deposited and annealed samples made from both 90 °C sol and 180 °C sol

It can be noticed that the values of the real part are higher than those of the imaginary part, they show similar spectral nature. Both the real and imaginary part of the dielectric constant, decrease in an exponential manner with wavelength. Since for our samples $n^2 >> k^2$, we can say that the real part of the dielectric constant mostly depends on n^2. Thus the spectral dependence of the real part of the dielectric constant show similar nature to that of refractive index. Imaginary part of the dielectric constant also exhibit same kind of spectral dependence. On application of external electric field due to space-charge polarization large numbers of dipole moments are created and trapped by defect states present in the films. When these defect states are thermally activated ionization process gets triggered increasing the imaginary part of the dielectric constant. A polycrystalline material is composed of several grains surrounded by their grain boundaries which provides a perfect place for accumulation of space charge. External thermal energy relaxes these grain boundaries allowing a larger number of charges to sit on. This contributes to the real part of dielectric constant. The improvement in crystal structure and the densification of the films after annealing also result in an increased dielectric constant.

We also evaluated the frequency dependence of the dielectric loss factor (tan δ) and are shown in figure 9. It is clearly seen that tanδ increases with increase in sol preparation temperature and annealing effect which indicate thermally activated relaxation in the material. the relaxation peaks were observed to shift slightly with the sol preparation temperature but not with annealing.

Figure 10 shows the PL spectra for annealed (at 500°C) and as-deposited films in the wavelength range 310 ─ 650 nm. In this range several well-resolved PL peaks ware observed. Similar nature of PL emission has also been reported by Abazović et al. for all the samples band edge transition was observed at 370 nm. Other peaks appear due to several kind of defect levels mostly related to the surface states and oxygen vacancies[53]. 398 nm and 415 nm peaks are the result of the charge-transfer transition from Ti^{3+} to oxygen anion in a TiO_6^{8-} complex. Zuo et al. also reported the presence of such kind of band associated with Ti^{3+} sites just below the

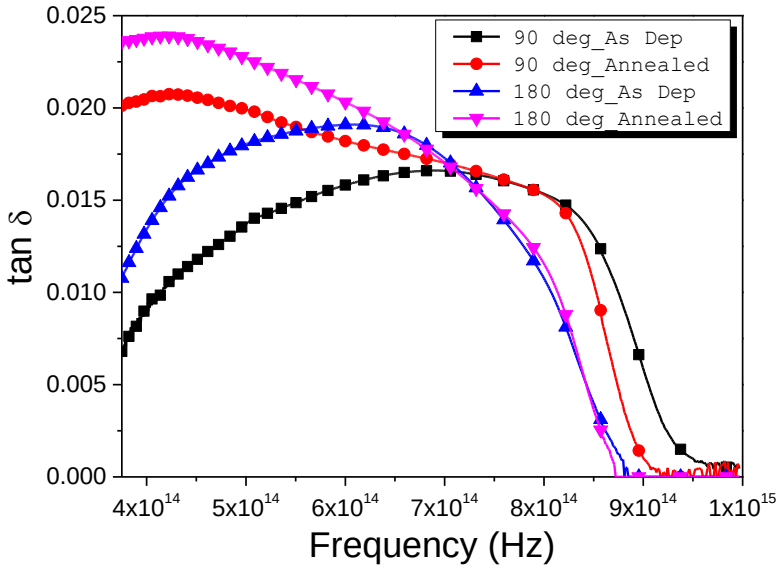

Figure 9: Dielectric Loss of as deposited and annealed samples made from both 90 °C sol and 180 °C sol

conduction band minima. Theoretical studies also supported the presence of these kind of bands. Transitions via charge carriers trapped at oxygen vacancies was observed at 442 nm. The emission bands at 452 nm and 473 nm for all the samples indicates the transition involving surface states and occurs due to the recombination of trapped electron–hole arising from unsaturated bonds in the TiO_2 nanoparticles on the surface. When some titanium atoms are exposed to the surface region of thin film and changed into Ti^{3+}, Ti^{2+}, Ti^{+}, localized energy levels are introduced within the forbidden gap. Several small peaks were observed in the wavelength range 460-560 nm. These peaks mainly result from the self-trapped excitons and oxygen vacancies. Due to the self trapping, excitons lose energy via lattice relaxation process and as a result, the PL peak is observed at higher wavelength region.

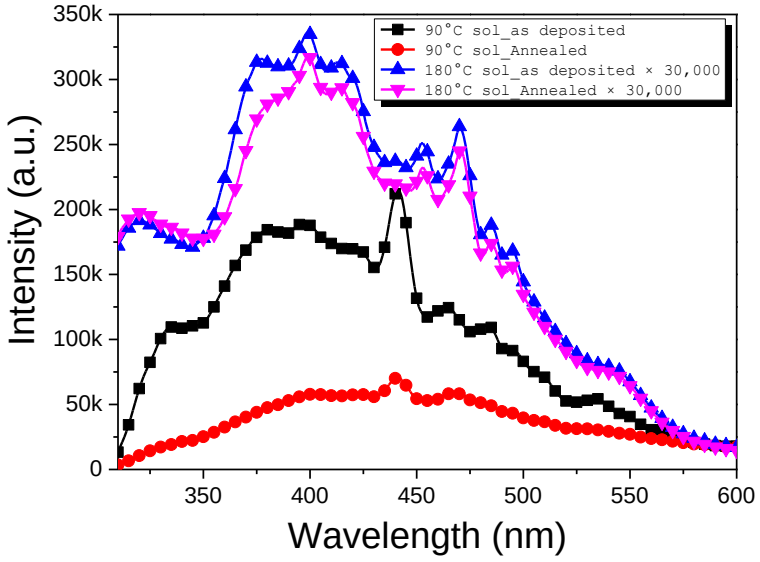

Figure 10: Photoluminescence emission spectra of (a) samples made from 90 °C sol and (b) samples made from 180 °C sol

PL intensity was found to decrease with increasing thickness. From XRD data we observed that, crystallite size (and the grain size as well) increases with increase in film thickness. In general, the density of the surface states decreases with the grain size increase and luminescence intensity decreases with decrease of the density of the surface states. FESEM images of our samples reveal that

TiO_2 particle size increases with increasing sol preparation temperature. With bigger particles present on the surface exposed surface area is also enhanced indicating the possibility of more and more dangling bonds. These bonds act as centres for non-radiative recombination and quenches the PL intensities. With more and more thermal energy provided to the films (both by annealing and increased sol preparation temperature), crystallinity improves, as supported by XRD data, which indicates towards the reduction of imperfections in the samples. This further decreases the intensity of the PL peaks. Since our samples were annealed in air, during annealing process, some of the oxygen vacant states are annihilated by capturing ambient oxygen and thus number of oxygen vacant defect states are reduced resulting in quench of PL intensities.

3.5 Photocatalytic Activity:

The photodegradation of Methylene Blue dye by TiO_2 photcatalysts is a pseudo-first-order reaction where the photodegradation rate constant (k) can be determined by the following equation:

$$ln\frac{C_t}{C_0} = -kt \quad (13)$$

Where C_0 and C_t are the initial concentration and the concentration at time t of the dye solution, respectively, and k is the first-order rate constant.

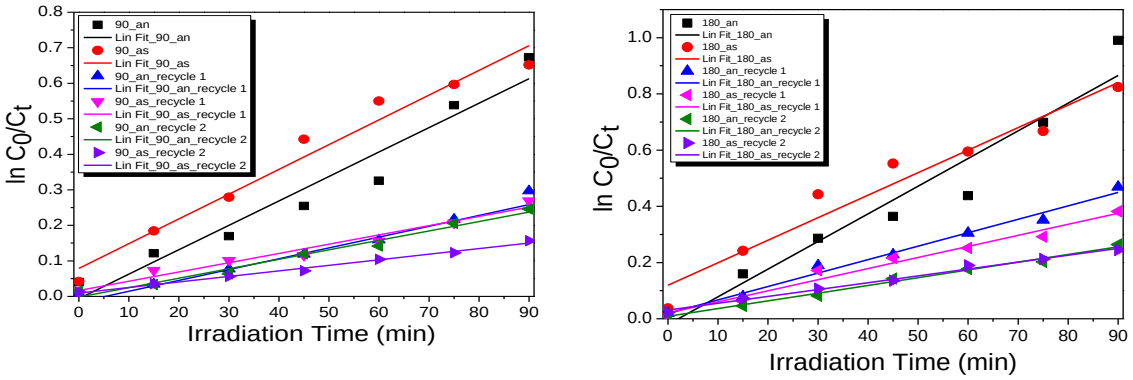

Figure 11: Determination of rate constant for photodegradation of dye with catalyst made from (a) 90 °C sol and (b) 180 °C sol

A plot of ln C0/Ct vs time represented in figure 11 yields a linear nature, slope of which upon linear regression determines the first-order rate constant k. Higher values of k indicates better degradation.

The degradation rate of the dye is generally expressed as,

$$\textbf{Degradation Rate} = \frac{C_0 - C_t}{C_0} \quad (14)$$

The photocatalytic activities of the prepared samples were observed to increase as the sol preparation temperature increases and also as a result of annealing. As deposited and annealed samples made from 180 °C sol degradation of dye was fond to be 56.1% and 62.8%. these values for samples made from the other sol is 47.9% and 49%. The absorbance spectra of the collected dye solutions are represented in figure 12. Degradation of the dye after 90 min and the kinetic rate for each sample has been represented in figure 13.

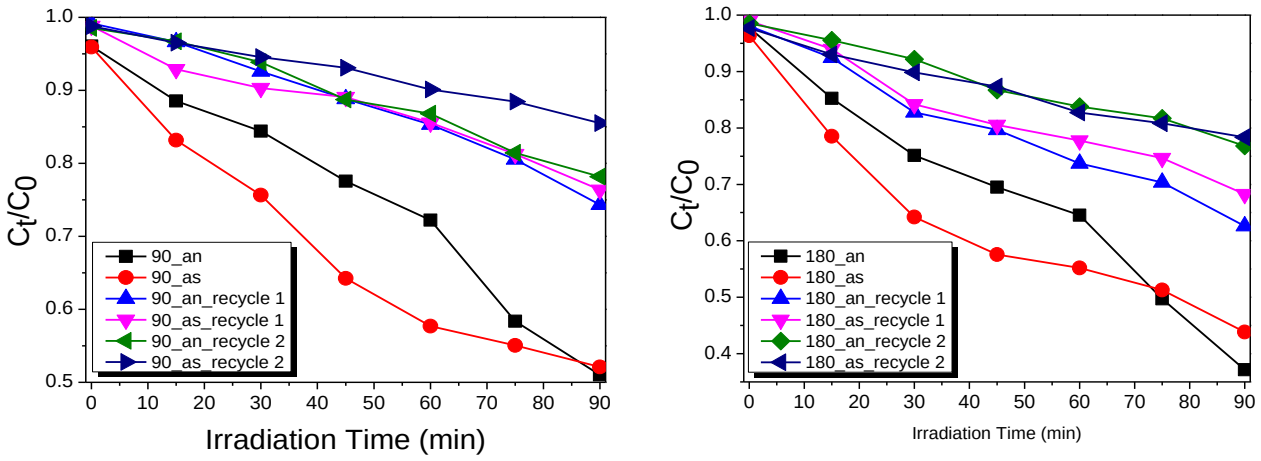

Figure 12: Photodegradation of dye with catalyst made from (a) 90 °C sol and (b) 180 °C sol

Enhancement in photocatalytic activity depends on effective separation of photo-induced e^-—h^+ pair in the dye material. PL intensities are indicative to amount of radiative recombination. For the present case PL intensity decreases with annealing and increase in sol preparation temperature suggestion a decrease in recombination of the e^-—h^+ pair. Thus increase in degradation rate for these samples is quite justified. FESEM images confirm increase in particle size for annealed samples and also for samples made with higher temperature sol. This provides additional effective surface area and consecutively more number of active sites available to enhance the degradation pathway and thus increasing the degradation rate.

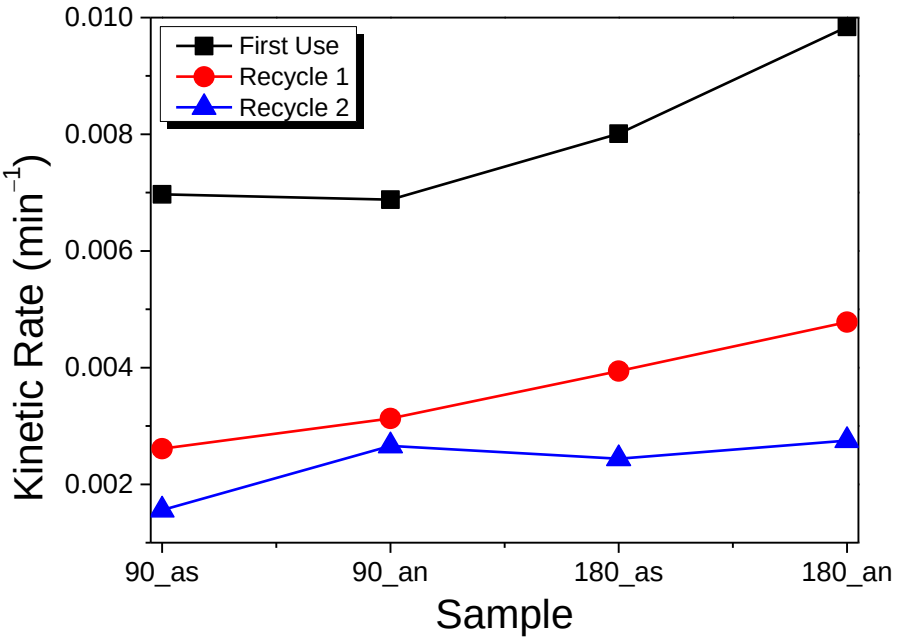

Figure 13: Kinetic rate of photodegradation of dye with photocatalysts made from 90 °C sol and 180 °C sol

To examine the stability of or photocatalyst we have repeated the photodegradation process with each of the prepared sample twice more and observed that when we use them for the second time (recycle 1) degradation rate drops a lot. At third use it decreases to around 20% at 90 min. The degradation of the dye (in %) after carrying out the photocatalysis process for 90 min is shown in figure 14.

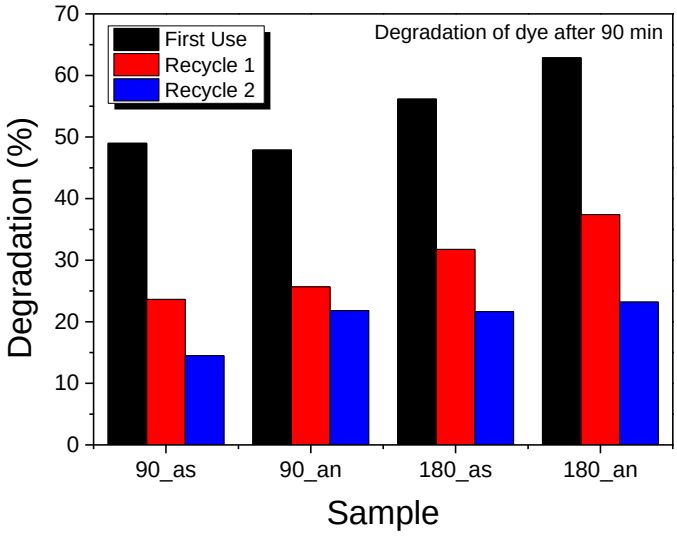

Figure 14: Degradation rate of dye solution with photocatalyst made from 90 °C sol and 180 °C sol

4. Conclusions

Anatase titania thin films were successfully prepared by hydrothermal assisted sol-gel dip coating method. The hydrothermal process to obtain the sol was carried out separately at two different temperatures, viz. 90 ºC and 180 ºC for 12 h each. For each hydrothermal temperature, samples were annealed at 500 ºC for 6h and also kept in as deposited condition. Both as deposited and annealed samples were crystallized in anatase phase and crystallite size was found to increase with increased sol preparation temperature and annealing as well. For samples prepared from 180 °C sol, the values are 16.8 nm and 18.3 nm for as deposited and anneald film respectively. For the same samples made from 180 °C sol the same are 13.9 nm and 17.4 nm. All the films consist of tiny spherical particles. Particle size increases with increasing sol preparation temperature. Annealing also imposes similar effect on the samples. Atomic force microscopy shows that, both RMS and average surface roughness increases with increased sol, preparation temperature and annealing in the similar manner. For samples prepared from 90 °C sol, RMS roughness was observed to be ~47 nm and ~22 nm for annealed and as-deposited samples respectively. For the similar kind of samples, the value increases to ~76 nm and ~34 nm when the sol preparation temperature is increased to 180 °C. In case of average roughness, values for the same samples are found to be ~37 nm, ~17 nm, ~60 nm and ~27 nm respectively. For all the samples RMS and average roughness maintain a constant ratio of 1.26. The prepared films exhibit almost zero transmittance at violet-ultraviolet transition region and then have a gradual rise in the visible region upto a maximum value of ~40% at the near Infrared. All the samples exhibit similar nature of transmitace. Transmittance value decreases as sol preparation temperature is increased and also due to annealing. Band gap values for all the samples do not show any significant difference before and after annealing. But when the sol preparation temperature increased, they exhibited a decreament due to quantum confinement. As result of improved crystallinity and greater packing density refractive index values were observed to increase with increase in sol preparation temperature and also with annealing. Extinction co-efficient also exhibited the behaviour. Since the real part of the dielectric constant mostly depends on n^2. Thus the spectral dependence of the real part of the dielectric constant show similar nature to that of refractive index. Dielectric loss (tanδ) increases with increase in sol preparation temperature and annealing effect indicating thermally activated relaxation of the created dipoles. Photoluminescence spectra show the appearance of several peaks in the wavelength range 350 ─ 550 nm. Most of the peaks are due to several surface defect states and defect levels related to oxygen vacancies. All the samples exhibit similar PL nature. Intensity of PL peaks gets quenched when samples were annealed and sol preparation temperature was higher because of annihilation oxygen vacant states by the ambient oxygen. Improved crystallinity diminishes number of imperfect sites in the films reducing the amount of radiative recombination of the electron-hole pair. And due to this annealed samples and those made from higher temperature sol showed higher photocatalytic activity.

Data accessibility:
The data will be available on request

Conflict of interest declaration:

There are no conflicts of interest

Acknowledgements.

Authors are grateful to Central Research Facility (CRF), IIT (ISM) Dhanbad for providing UV-Vis NIR spectroscopy, FESEM and AFM facility. We also acknowledge DST-FIST facility (project no. SR/FST/PSI-004/2013) for using photoluminescence spectrometer facility.

References

1. Hagfeldt, A., Boschloo, G., Sun, L., Kloo, L., & Pettersson, H. (2010). Dye-sensitized solar cells. *Chemical reviews*, *110*(11), 6595-6663.

2. Jung, H. S., & Lee, J. K. (2013). Dye sensitized solar cells for economically viable photovoltaic systems. *The journal of physical chemistry letters*, *4*(10), 1682-1693.

3. O'regan, B., & Grätzel, M. (1991). A low-cost, high-efficiency solar cell based on dye-sensitized colloidal TiO2 films. *nature*, *353*(6346), 737-740.

4. Tachikawa, T., Fujitsuka, M., & Majima, T. (2007). Mechanistic insight into the TiO2 photocatalytic reactions: design of new photocatalysts. *The Journal of Physical Chemistry C*, *111*(14), 5259-5275.

5. Kadoshima M., Hiratani M., Shimamoto Y., Torii K., Miki H., Kimura S., & Nabatame T., Thin Solid Films, 2003, 424(2), 224-228.

6. Wang, J., Polleux, J., Lim, J., & Dunn, B. (2007). Pseudocapacitive contributions to electrochemical energy storage in TiO2 (anatase) nanoparticles. *The Journal of Physical Chemistry C*, *111*(40), 14925-14931.

7. Ochiai, T., & Fujishima, A. (2012). Photoelectrochemical properties of TiO2 photocatalyst and its applications for environmental purification. Journal of Photochemistry and photobiology C: Photochemistry reviews, 13(4), 247-262.

8. Khan, S. U., Al-Shahry, M., & Ingler, W. B. (2002). Efficient photochemical water splitting by a chemically modified n-TiO2 Science, 297(5590), 2243-2245.

9. Lu H. F., Li, F., Liu G., Chen, Z. G., Wang D. W., Fang H. T. & Cheng H. M., Nanotechnology, 2008, 19(40), 405504.

10. Kwon, D. H., Kim, K. M., Jang, J. H., Jeon, J. M., Lee, M. H., Kim, G. H., ... & Kim, M. (2010). Atomic structure of conducting nanofilaments in TiO2 resistive switching memory. Nature nanotechnology, 5(2), 148-153.

11. Jeong, H. Y., Lee, J. Y., & Choi, S. Y. (2010). Interface-Engineered Amorphous TiO2-Based Resistive Memory Devices. Advanced Functional Materials, 20(22), 3912-3917.

12. Braun, J. H., Baidins, A., & Marganski, R. E. (1992). TiO2 pigment technology: a review. Progress in organic coatings, 20(2), 105-138

13. Huang, J., Shinohara, T., & Tsujikawa, S. (1999). Protection of carbon steel from atmospheric corrosion by TiO2 coating. Zairyo-to-Kankyo, 48(9), 575-582

14. Richards, B. S. (2003). Single-material TiO2 double-layer antireflection coatings. Solar Energy Materials and Solar Cells, 79(3), 369-390.

15. Leprince-Wang, Y., & Yu-Zhang, K. (2001). Study of the growth morphology of TiO2 thin films by AFM and TEM. *Surface and Coatings Technology*, *140*(2), 155-160.

16. Bennett, J. M., Pelletier, E., Albrand, G., Borgogno, J. P., Lazarides, B., Carniglia, C. K., ... & Saxer, A. (1989). Comparison of the properties of titanium dioxide films prepared by various techniques. *Applied optics*, *28*(16), 3303-3317.

17. Chen, J. S., Chao, S., Kao, J. S., Lai, G. R., & Wang, W. H. (1997). Substrate-dependent optical absorption characteristics of titanium dioxide thin films. *Applied optics*, *36*(19), 4403-4408.

18. M. Laube et. al., Physics Research Section B: Beam Interactions with Materials and Atoms, 113(1-4), 1996, 288-292

19. H.K. Pulker et. al., Applied optics, 15(12), 1976, 2986-2991

20. Negishi, N., Iyoda, T., Hashimoto, K., & Fujishima, A. (1995). Preparation of transparent TiO2 thin film photocatalyst and its photocatalytic activity. Chemistry Letters, 24(9), 841-842.

21. Kasuga, T., Hiramatsu, M., Hoson, A., Sekino, T., & Niihara, K. (1998). Formation of titanium oxide nanotube. Langmuir, 14(12), 3160-3163.

22. Pore, V., Rahtu, A., Leskelä, M., Ritala, M., Sajavaara, T., & Keinonen, J. (2004). Atomic layer deposition of photocatalytic TiO2 thin films from titanium tetramethoxide and water. Chemical Vapor Deposition, 10(3), 143-148.

23. Besserguenev, V. G., Pereira, R. J. F., Mateus, M. C., Khmelinskii, I. V., Nicula, R. C., & Burkel, E. (2003). TiO2 thin film synthesis from complex precursors by CVD, its physical and photocatalytic properties. International Journal of Photoenergy, 5(2), 99-105.

24. Mohamed, F. N., Rahim, M. S. A., Nayan, N., Ahmad, M. K., Sahdan, M. Z., & Lias, J. (2015). *Influence of TiO2 Thin Film Annealing Temperature on Electrical Properties Sythesized by CVD Technique* (Doctoral dissertation, Universiti Tun Hussein Onn Malaysia).

25. Karuppuchamy, S., Nonomura, K., Yoshida, T., Sugiura, T., & Minoura, H. (2002). Cathodic electrodeposition of oxide semiconductor thin films and their application to dye-sensitized solar cells. Solid State Ionics, 151(1), 19-27.
26. Ichinose, H., Terasaki, M., & Katsuki, H. (2001). Properties of peroxotitanium acid solution and peroxo-modified anatase sol derived from peroxotitanium hydrate. Journal of Sol-Gel Science and Technology, 22(1), 33-40.
27. Lee, C. K., Kim, D. K., Lee, J. H., Sung, J. H., Kim, I., Lee, K. H., ... & Lee, Y. K. (2004). Preparation and characterization of peroxo titanic acid solution using TiCl 3. Journal of sol-gel science and technology, 31(1), 67-72.
28. Ge, L., Xu, M., Fang, H., & Sun, M. (2006). Preparation of TiO 2 thin films from autoclaved sol containing needle-like anatase crystals. Applied Surface Science, 253(2), 720-725.
29. Nadzirah, S., & Hashim, U. (2013, September). Effects of annealing temperature on current-voltage characteristics of TiO 2 thin film by sol-gel process on silicon substrate for biosensor application. In *RSM 2013 IEEE Regional Symposium on Micro and Nanoelectronics* (pp. 167-170). IEEE.
30. Yuan, J., & Tsujikawa, S. (1995). Characterization of sol-gel-derived TiO2 coatings and their photoeffects on copper substrates. *Journal of the Electrochemical Society*, *142*(10), 3444.
31. Niesen, T. P., Bill, J., & Aldinger, F. (2001). Deposition of titania thin films by a peroxide route on different functionalized organic self-assembled monolayers. *Chemistry of materials*, *13*(5), 1552-1559.
32. Dutta, S., Leeladhar, L., Pandey, A., Thakur, O. P., & Pal, R. (2015). Electrical properties of ultrathin titanium dioxide films on silicon. *Journal of Vacuum Science & Technology A*, *33*(2).
33. Kim, D. J., Hahn, S. H., Oh, S. H., & Kim, E. J. (2002). Influence of calcination temperature on structural and optical properties of TiO2 thin films prepared by sol–gel dip coating. *Materials Letters*, *57*(2), 355-360.
34. Takahashi, Y., & Matsuoka, Y. (1988). Dip-coating of TiO 2 films using a sol derived from Ti (O-i-Pr) 4-diethanolamine-H 2 O-i-PrOH system. *Journal of Materials Science*, *23*, 2259-2266.
35. Karuppasamy, A., & Subrahmanyam, A. (2007). Studies on the room temperature growth of nanoanatase phase TiO2 thin films by pulsed dc magnetron with oxygen as sputter gas. *Journal of Applied Physics*, *101*(6).
36. Wang, T. M., Zheng, S. K., Hao, W. C., & Wang, C. (2002). Studies on photocatalytic activity and transmittance spectra of TiO2 thin films prepared by rf magnetron sputtering method. *Surface and Coatings Technology*, *155*(2-3), 141-145.
37. Karuppasamy, A., & Subrahmanyam, A. (2007). Studies on the room temperature growth of nanoanatase phase TiO2 thin films by pulsed dc magnetron with oxygen as sputter gas. *Journal of Applied Physics*, *101*(6).
38. Gadelmawla, E. S., Koura, M. M., Maksoud, T. M. A., Elewa, I. M., & Soliman, H. H. (2002). Roughness parameters. *Journal of Materials Processing Technology*, *123*(1), 133-145.
39. Wang, M., Wang, J., Chen, W., Cui, Y., & Wang, L. (2006). Effect of preheating and annealing temperatures on quality characteristics of ZnO thin film prepared by sol–gel method. *Materials Chemistry and Physics*, *97*(2-3), 219-225.
40. Liu, Y. C., Tung, S. K., & Hsieh, J. H. (2006). Influence of annealing on optical properties and surface structure of ZnO thin films. *Journal of crystal growth*, *287*(1), 105-111.
41. Lin, Y., Xie, J., Wang, H., Li, Y., Chavez, C., Lee, S., ... & Jia, Q. X. (2005). Green luminescent zinc oxide films prepared by polymer-assisted deposition with rapid thermal process. *Thin Solid Films*, *492*(1-2), 101-104.
42. Arthanarieswaran, V. P., Kumaravel, A., & Saravanakumar, S. S. (2015). Physico-chemical properties of alkali-treated Acacia leucophloea fibers. *International Journal of Polymer Analysis and Characterization*, *20*(8), 704-713.
43. Kumar, B. R., & Rao, T. S. (2012). AFM studies on surface morphology, topography and texture of nanostructured zinc aluminum oxide thin films. *Digest Journal of Nanomaterials and Biostructures*, *7*(4), 1881-1889.
44. H.C. Ward, Rough Surfaces, T.R. Thomas Ed., Longman, London (1982).
45. Li, L., Chen, W., Zheng, J., Wang, L., & Chen, Y. (2016). Characterization of silver nanoparticles thin films with various thicknesses by AFM. *Journal of Materials Science and Chemical Engineering*, *4*(1), 34-39.
46. Lekshmy, S. S., Daniel, G. P., & Joy, K. (2013). Microstructure and physical properties of sol gel derived SnO2: Sb thin films for optoelectronic applications. *Applied Surface Science*, *274*, 95-100.
47. Williamson, G. K., & Smallman, R. E. (1956). III. Dislocation densities in some annealed and cold-worked metals from measurements on the X-ray debye-scherrer spectrum. *Philosophical magazine*, *1*(1), 34-46.
48. Shei, S. C. (2013). Optical and structural properties of titanium dioxide films from TiO2 and Ti3O5 starting materials annealed at various temperatures. *Advances in Materials Science and Engineering*, *2013*(1), 545076.
49. Zhang, F., Zheng, Z., Ding, X., Mao, Y., Chen, Y., Zhou, Z., ... & Liu, X. (1997). Highly oriented rutile-type TiO 2 films synthesized

by ion beam enhanced deposition. *Journal of Vacuum Science & Technology A: Vacuum, Surfaces, and Films*, *15*(4), 1824-1827.
50. Fujii, T., Sakata, N., Takada, J., Miura, Y., Daitoh, Y., & Takano, M. (1994). Characteristics of titanium oxide films deposited by an activated reactive evaporation method. *Journal of materials research*, *9*(6), 1468-1473.
51. N. A. Subrahamanyam: A Text Book of Optics, Ninth ed., BRJ Laboratoray Delhi, India 1977.
52. Eckortova L., "Physics of Thin Films ", (plenum press) (1977).
53. Liu, B., Zhao, X., & Wen, L. (2006). The structural and photoluminescence studies related to the surface of the TiO 2 sol prepared by wet chemical method. Materials Science and Engineering: B, 134(1), 27-31.